
ASSESSING DIFFERENTIALLY PRIVATE DEEP LEARNING WITH MEMBERSHIP INFERENCE

PREPRINT

Daniel Bernau, Philip-William Grassal*, Jonas Robl*
SAP SE
Karlsruhe, Germany
firstname.lastname@sap.com

Florian Kerschbaum
University of Waterloo
Waterloo, Canada
florian.kerschbaum@uwaterloo.ca

December 9, 2021

ABSTRACT

Releasing data in the form of trained deep neural networks with differential privacy promises meaningful anonymization. However, there is an inherent privacy-accuracy trade-off in differential privacy which is challenging to assess for non-privacy experts. Moreover, local and central differential privacy mechanisms are available to either anonymize the training data or the learnt neural network, and the privacy parameter ϵ cannot be used to compare these two mechanism categories. We propose to measure privacy by a membership inference attack, and compare the privacy-accuracy trade-off for different local and central differential privacy mechanisms. Furthermore, we evaluate whether differential privacy is a useful mechanism against membership inference in practice since differential privacy will especially be used by data scientists if membership inference precision and recall are lowered more than neural network accuracy. We experiment with several datasets and show that neither local differential privacy nor central differential privacy yields a consistently better privacy-accuracy trade-off among all datasets. We also show that the relative privacy-accuracy trade-off is not strictly declining over ϵ and only favorable within a small interval. For this purpose, we propose φ , a ratio expressing the relative privacy-accuracy trade-off.

Keywords Machine Learning, Privacy

1 Introduction

Deep neural networks have successfully been applied to a wide range of learning tasks, each requiring its own specific set of training data, architecture and hyperparameters to achieve meaningful classification accuracy and foster generalization. In some learning tasks data scientists have to deal with personally identifiable or sensitive information, which results in two challenges. First, legal restrictions might not permit collecting, processing and publishing certain data, such as National Health Service data [4]. Second, membership inference [15, 28] and model inversion attacks [11, 30] are capable of identifying and reconstructing training data based on information leakage from a trained, published neural network. A mitigation to both challenges is offered by anonymized deep neural network training with differential privacy. However, a data scientist has the choice between two differential privacy (DP) mechanism categories: local differential privacy (LDP) [31] and central differential privacy (CDP) [7]. The two mechanism categories either perturb the training data (i.e., LDP) before any processing takes place or the gradient update steps during training (i.e., CDP). The degree of perturbation, which affects the accuracy of the trained neural network on test data, is calibrated for both DP categories by adjusting their respective privacy parameter ϵ . Choosing ϵ too large will unlikely mitigate privacy attacks such as membership inference, or vice versa significantly erode model accuracy. Thus, balancing the privacy-accuracy trade-off is an inherent problem especially for data scientists who are not experts in DP.

The reasons mentioned above might lead data scientists to generally rule out LDP when designing differentially private neural networks due to accuracy and privacy concerns raised by the comparatively higher privacy parameter ϵ in LDP.

*Both authors contributed equally.

In this work, we compare the privacy parameter ϵ by applying the MI attack of Shokri et al. [28] in LDP and CDP settings for learning problems from diverse domains: consumer matrices, social graphs, face recognition and health data. This methodology allows us to compare between LDP and CDP in terms of the privacy-accuracy trade-off, and to support data scientists in selecting DP mechanisms and privacy parameters.

In summary, this work makes the following contributions:

- We compare LDP and CDP based on MI precision and recall as privacy measures and show that under these measures they have similar privacy-accuracy trade-offs despite vastly different privacy parameters ϵ . We provide extensive evaluation on various datasets and reference models, such as face and graph data.
- We show that CDP mechanisms are not achieving a consistently better privacy-accuracy trade-off. This trade-off rather depends on the specific dataset at hand.
- We analyze the relative privacy-accuracy trade-off and show that it is not linear over ϵ , but that for each data set there are ranges where the relative trade-off is most favorable. The relative privacy-accuracy trade-off allows discussing choices of ϵ w.r.t. points at which the effect of ϵ on MI precision and recall stagnates, and identifying efficient privacy regimes in which MI precision and recall are lowered more than test accuracy.

The remainder of this paper is structured as follows: In Section 2 we outline the use of local and central differential privacy in the data science process for deep learning. We suggest comparing privacy guarantees under a membership inference threat model, which we revisit in Section 3. We introduce and analyze experiments and datasets in Section 4 and 5. We discuss our findings in Section 6. We provide related work and conclusions in Section 7 and 8.

2 Differential Privacy

In contrast to anonymization methods based on generalization, DP [6] anonymizes a dataset $\mathcal{D} = \{d_1, \dots, d_n\}$ by perturbation. DP can be either enforced locally to each entry $d \in \mathcal{D}$, or centrally to an aggregation function $f(\mathcal{D})$.

2.1 Central DP

In the central model the aggregation function $f(\cdot)$ is evaluated and perturbed by a trusted server. Due to perturbation it is no longer possible for an adversary to confidently determine whether $f(\cdot)$ was evaluated on \mathcal{D} , or some neighboring dataset \mathcal{D}' differing in one element. Thus, assuming that every participant is represented by one element, privacy is provided to participants in \mathcal{D} as their impact of presence (absence) on $f(\cdot)$ is limited. *Mechanisms* \mathcal{M} fulfilling Definition 1 are used for perturbation of $f(\cdot)$ [7]. We refer to the application of a mechanism \mathcal{M} to a function $f(\cdot)$ as *central differential privacy*.

Definition 1 ((ϵ, δ)-central differential privacy) *A mechanism \mathcal{M} gives (ϵ, δ)-central differential privacy if $\mathcal{D}, \mathcal{D}' \subseteq \text{DOM}$ differing in at most one element, and all outputs $\mathcal{S} \subseteq \mathcal{R}$*

$$\Pr[\mathcal{M}(\mathcal{D}) \in \mathcal{S}] \leq e^\epsilon \cdot \Pr[\mathcal{M}(\mathcal{D}') \in \mathcal{S}] + \delta$$

CDP holds for all possible differences $\|f(\mathcal{D}) - f(\mathcal{D}')\|_2$ by adapting to the global sensitivity of $f(\cdot)$ per Definition 2.

Definition 2 (Global ℓ_2 Sensitivity) *Let \mathcal{D} and \mathcal{D}' be neighboring. The global ℓ_2 sensitivity of a function f , denoted by Δf , is defined as*

$$\Delta f = \max_{\mathcal{D}, \mathcal{D}'} \|f(\mathcal{D}) - f(\mathcal{D}')\|_2.$$

To enforce CDP in deep learning we use differentially private versions of two standard gradient optimizers: SGD and Adam². We refer to these CDP optimizers as DP-SGD and DP-Adam. A differentially private optimizer represents a differentially private training mechanism \mathcal{M}_{nn} that updates the weight coefficients θ_t of a neural network per training step $t \in T$ with $\theta_t \leftarrow \theta_{t-1} - \alpha(\tilde{g})$, where $\tilde{g} = \mathcal{M}_{nn}(\partial \text{loss} / \partial \theta_{t-1})$ denotes a Gaussian perturbed gradient and α is some scaling function on \tilde{g} to compute an update, i.e., learning rate or running moment estimations. Differentially private noise is added by the Gaussian mechanism of Definition 3 as suggested by Abadi et al. [1].

²The Tensorflow privacy package was used throughout this work: <https://github.com/tensorflow/privacy>.

Definition 3 (Gaussian Mechanism [8])

Let $\epsilon \in (0, 1)$ be arbitrary. For $c^2 > 2\ln(\frac{1.25}{\delta})$, the Gaussian mechanism with parameter $\sigma \geq c\frac{\Delta f}{\epsilon}$ gives (ϵ, δ) -CDP, adding noise scaled to $\mathcal{N}(0, \sigma^2)$.

After T update steps, \mathcal{M}_{nn} outputs a differentially private weight matrix θ which is used by the prediction function $h(\cdot)$ of a neural network. A CDP gradient optimizer bounds the sensitivity of the computed gradients by a clipping norm C based on which the gradients get clipped before perturbation.

Since weight updates are performed iteratively during training, a composition of \mathcal{M}_{nn} is required until the the training step T is reached and the final private weights θ are obtained. For CDP we measure privacy decay under composition by tracking the noise levels σ we used to invoke the Gaussian mechanism. After training we transform and compose σ under Renyi differential privacy [21], and transform the aggregate again to CDP. We chose this accumulation method over other advanced composition schemes (e.g., Advanced Composition or Moments Accountant [18, 1]) since it provides tighter bounds for heterogeneous mechanism invocations.

2.2 Local DP

We refer to the perturbation of entries $d \in \mathcal{D}$ as local differential privacy [31]. LDP is the standard choice when the server by which evaluates a function $f(D)$ is untrusted. We adapt the definitions of Kasiviswanathan et al. [19] to achieve LDP by using local randomizers \mathcal{LR} .

Definition 4 (Local differential privacy) A local randomizer (mechanism) $\mathcal{LR} : \mathcal{DOM} \rightarrow \mathcal{S}$ is ϵ -local differentially private, if $\epsilon \geq 0$ and for all possible inputs $v, v' \in \mathcal{DOM}$ and all possible outcomes $s \in \mathcal{S}$ of \mathcal{LR}

$$\Pr[\mathcal{LR}(v) = s] \leq e^\epsilon \cdot \Pr[\mathcal{LR}(v') = s]$$

In the experiments within this work we use a local randomizer to perturb each record $d \in \mathcal{D}$ independently. Since a record may contain multiple correlated features (e.g., pixels in an image, items in a preference vector) a local randomizer must be applied repeatedly which results in a sequentially increasing loss of privacy. A series of local randomizer executions per record composes a local algorithm according to Definition 5. ϵ -local algorithms are ϵ -local differentially private [19], where ϵ is a summation of all composed local randomizer guarantees.

Definition 5 (Local Algorithm) An algorithm is ϵ -local if it accesses the database \mathcal{D} via \mathcal{LR} with the following restriction: for all $i \in \{1, \dots, |\mathcal{D}|\}$, if $\mathcal{LR}_1(i), \dots, \mathcal{LR}_k(i)$ are the algorithms invocations of \mathcal{LR} on index i , where each \mathcal{LR}_j is an ϵ_j -local randomizer, then $\epsilon_1 + \dots + \epsilon_k \leq \epsilon$.

We perturb low domain data with randomized response [32], a (composed) local randomizer. According to Equation (1) randomized response yields $\epsilon = \ln(3)$ LDP for a one-time collection of values from binary domains (e.g., {yes, no}) with two fair coins [9]. That is, retention of the original value with probability $\rho = 0.5$ and uniform sampling with probability $(1 - \rho) \cdot \rho$.

$$\epsilon = \ln \left(\frac{\rho + (1 - \rho) \cdot \rho}{(1 - \rho)^2} \right) = \ln \left(\frac{\Pr[\text{yes}|\text{yes}]}{\Pr[\text{yes}|\text{no}]} \right). \quad (1)$$

In our evaluation we also look at image data for which we rely on the local randomizer by Fan [10] for LDP image pixelation. The randomizer applies the Laplace mechanism of Definition 6 with scale $\lambda = \frac{255 \cdot m}{b^2 \cdot \epsilon}$ to each pixel. Parameter m represents the neighborhood in which LDP is provided. Full neighborhood for an image dataset would require that any picture can become any other picture. As a rule of thumb providing DP within large neighborhood will require high ϵ values to retain meaningful image structure, and vice versa. High privacy will result in uniform random black and white images.

Definition 6 (Laplace Mechanism [8]) Given a numerical query function $f : \mathcal{DOM} \rightarrow \mathbb{R}^k$, the Laplace mechanism with parameter $\lambda = \frac{\Delta f}{\epsilon}$ is an ϵ -differentially private mechanism, adding noise scaled to $\text{Lap}(\lambda, \mu = 0)$.

Within this work we consider the use of LDP and CDP for deep learning along a generic data science process (e.g., CRISP-DM [33]). In such processes a process the dataset \mathcal{D} of a data owner \mathcal{DO} is (i) transformed, and (ii) used to learn a model function $h(\cdot)$ (e.g., classification), which (iii) afterwards is deployed for evaluation by third parties. In the following $h(\cdot)$ will represent a neural network. DP is applicable at every stage in the data science process. In the form of LDP by perturbing each record $d \in \mathcal{D}$, while learning $h(\cdot)$ centrally with a CDP gradient optimizer, or to the evaluation

Table 1: Notations and context

Symbol	Description
X	Set of vectors $\mathbf{x}_1, \dots, \mathbf{x}_j$ where x_j^1, \dots, x_j^i denote attribute values (<i>features</i>) of \mathbf{x}_j .
Y	Set of k target variables y_1, \dots, y_k (<i>labels</i>).
\mathbf{c}	$ Y $.
\mathbf{y}	Vector of target variables (<i>labels</i>) where variable $y_j \in \mathbf{y}$ represents the label for $\mathbf{x}_j \in X$.
\hat{y}	Predicted target variable, i.e., $\hat{y} = h(\mathbf{x})$.
$p(\mathbf{x})$	Softmax confidence for \mathbf{x} .
\mathcal{D}	$\mathcal{D} := (X, \mathbf{y})$.
d	A record $d \in \mathcal{D}$, where $d := (\mathbf{x}, y)$.
n	$ \mathcal{D}_{\text{target}}^{\text{train}} $.

of $h(\cdot)$ by federated learning with CDP voting [23]. We focus on the data science process without collaboration and keep federated learning for future reference.

When applying DP in the data science process the privacy-accuracy trade-off is of particular interest. Similar to the evaluation of regularization techniques that apply noise to the training data to foster generalization (e.g., [13, 14, 20]) we judge utility by the test accuracy of $h(\cdot)$. I.e., the accuracy of $h(\cdot)$ on test data after having learned $h(\cdot)$ from training data.

3 Membership Inference

MI attacks aim at identifying the presence of an individual record d by exploiting the information leakage of a machine learning model trained on dataset \mathcal{D} . While several MI attacks have been formulated (cf. Section 7) this paper solely refers to the black-box MI attack against machine learning models by Shokri et al [28]. Throughout this section we will first outline the MI attack and, second, illustrate how the attack is used to assess LDP and CDP privacy parameters. We use a set of notations that is summarized in Table 1.

3.1 Black-Box MI Attack

The black-box MI attack assumes an honest-but-curious Adversary \mathcal{A} with access to a trained prediction function $h(\cdot)$ and predictions from $h(\cdot)$ (e.g., softmax confidence values). We refer to the trained ML model against which the MI attack is applied as *target model*. Within three steps the MI attack exploits that an ML classifier such as a neural network tends to classify a record d from the model’s training dataset $\mathcal{D}_{\text{target}}^{\text{train}}$ with differing softmax confidence $p(\mathbf{x})|h(\mathbf{x})$ to its true label y in comparison to a record $d \notin \mathcal{D}_{\text{target}}^{\text{train}}$.

First, data owner \mathcal{DO} trains a ML model, *target model*, for some classification task with records from a dataset $\mathcal{D}_{\text{target}}^{\text{train}}$. After training \mathcal{DO} exposes the target model to the adversary \mathcal{A} for inference tasks, e.g., through an API. Second, \mathcal{A} trains copies of the target model w.r.t. structure and hyper-parameters, so called *shadow models*, on data statistically similar to $\mathcal{D}_{\text{target}}^{\text{train}}$. It applies that $|\mathcal{D}_{\text{shadow}_i}^{\text{train}}| = |\mathcal{D}_{\text{shadow}_i}^{\text{test}}| \wedge \mathcal{D}_{\text{shadow}_i}^{\text{train}} \cap \mathcal{D}_{\text{shadow}_i}^{\text{test}} = \emptyset \wedge |\mathcal{D}_{\text{shadow}_i}^{\text{train}} \cap \mathcal{D}_{\text{shadow}_j}^{\text{test}}| \geq 0$ for any $i \neq j$. After training, each shadow model is invoked by \mathcal{A} to classify all respective training and test data, i.e., $p(\mathbf{x})$, $\forall d \in \mathcal{D}_{\text{shadow}_i}^{\text{train}} \cup \mathcal{D}_{\text{shadow}_i}^{\text{test}}$. Since \mathcal{A} has full control over $\mathcal{D}_{\text{shadow}_i}^{\text{train}}$ and $\mathcal{D}_{\text{shadow}_i}^{\text{test}}$, each shadow model’s output $(p(\mathbf{x}), y)$ is appended with a label “in” if the corresponding record $d \in \mathcal{D}_{\text{shadow}_i}^{\text{train}}$. Otherwise, its label is “out”. Third, a binary classifier, *attack model*, is trained by \mathcal{A} per target variable $y \in Y$ to map $p(\mathbf{x})$ to the indicator “in” or “out”. The triples $(p(\mathbf{x}), y, \text{in/out})$ serve as attack model training data, i.e., $\mathcal{D}_{\text{attack}}^{\text{train}}$. The attack model thus exploits the imbalance between predictions on $d \in \mathcal{D}_{\text{target}}^{\text{train}}$ and $d \notin \mathcal{D}_{\text{target}}^{\text{train}}$.

Finally, the attack model is evaluated on tuples $(p(\mathbf{x}), \hat{y}) \forall d \in \mathcal{D}_{\text{target}}^{\text{train}}$, which simulates the worst case where \mathcal{A} tests membership for all training records.

We find the black-box MI attack to be especially effective when some classes within the training data comprise a comparatively low number of records and the overall training data distribution is imbalanced. We observed these

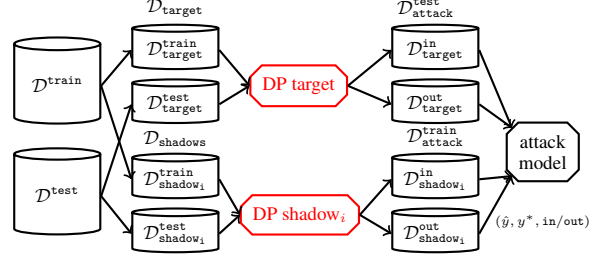


Figure 1: MI under central DP with DP gradient optimizer.

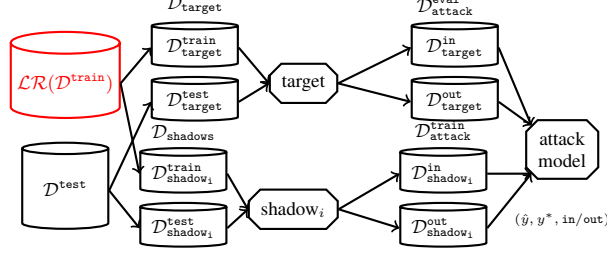


Figure 2: MI against LDP in target model training

imbalanced classes especially when learning models from sensitive or personal training data, such as the Labeled Faces in the Wild or Texas Hospital Stays datasets which we introduce in Section 4.

3.2 Evaluating CDP and LDP under MI

Considering that both DP and MI are tailored to the protection and identification of individual data records we argue for evaluating DP privacy by MI Attack precision and recall within this work and focus on two privacy questions: “How many records predicted as in are truly contained in the training dataset?” (precision), and “How many truly contained records are predicted as in?” (recall). We calculate \mathcal{A} ’s MI precision and recall as the average score over the instances of all classes to ensure comparability to the results of Shokri et al. [28].

We illustrated that \mathcal{DO} has two options to apply DP within the data science process. Either LDP by applying a local randomizer on the training data and using the resulting $\mathcal{LR}(\mathcal{D}^{\text{train}}_{\text{target}})$ for training, or central DP with a differentially private optimizer on $\mathcal{D}^{\text{train}}_{\text{target}}$. A discussion and comparison limited to the privacy parameter ϵ likely falls short and potentially leads data scientists to incorrect conclusions. Thus, data scientists give up flexibility w.r.t. applicable learning algorithms and may miss a favorable privacy-accuracy trade-off, if they rule out the use of LDP due to comparatively greater ϵ and instead solely investigate CDP (e.g., DP-SGD). Instead we suggest to compare LDP and CDP by their concrete effect on an MI attack. While we consider the MI attack of Shokri et al. [28] our methodology is applicable to other MI attacks as well. Depending on the notion of privacy, the MI attack scheme described earlier in this section changes slightly. When examining CDP, we train both target and shadow models on the same datasets as would be used without any anonymization. However, a similar configured CDP optimizer is used during the training phase for target and shadow models. Adversary \mathcal{A} obtains higher MI precision and recall when relying on an equally configured DP optimizer for shadow model training, compared to use of the non-DP optimizer for shadow model training. The LDP setup requires a local randomizer to perturb the training inputs for both target and shadow models. See Figure 1 and Figure 2 for comparison.

We calculate the relative privacy-accuracy trade-off for LDP and CDP as the relative difference between \mathcal{DO} ’s change in test accuracy to the change in MI precision and recall, and introduce a measure for quantification in the following. Efficient privacy-accuracy trade-offs in LDP or CDP must reduce \mathcal{A} ’s susceptibility without sacrificing significant test accuracy for \mathcal{DO} . In the following we define our measure w.r.t. MI precision. However, the definition is analogously applicable to MI recall, and will be used for MI precision and recall throughout this work.

Let $prec_{orig}$ be \mathcal{A} ’s MI precision and acc_{orig} be \mathcal{DO} ’s original test accuracy, and let $prec_{\epsilon}$ be \mathcal{A} ’s MI precision and acc_{ϵ} be \mathcal{DO} ’s resulting test accuracy after application of LDP or CDP. Also, let acc_{base} be the minimal test accuracy of $1/C$ and $prec_{base}$ be the minimal MI precision of 0.5 (e.g., random guessing). For the calculation of φ we will clip decreases below the baseline since these indicate an Adversary worse than random guessing. Normalizing yields

Table 2: Overview of datasets considered in evaluation.

Dataset	Description	Model	Learning task
Texas Hospital Stays [28]	Unbalanced dataset. Per $C \in \{100, 150, 200, 300\}$ the dataset comprises 67, 330 records and 6, 170 features, 73, 032 records and 6, 382 features, 82, 243 records and 6, 382 features, and 89, 815 records with 6, 382 features.	Fully connected NN with three layers ($512 \times 128 \times C$) [28].	Predict patient’s main procedure from the $C \in \{100, 150, 200, 300\}$ most frequent procedures. We do not try to re-identify a known individual, and fully comply with the data use agreement for the original public use data file.
Purchases Shopping Carts [28]	Balanced dataset. Per $C \in \{10, 20, 50, 100\}$ the dataset comprises 200, 000 records and 600 features	Fully connected NN with two layers ($128 \times C$) [28].	Classify purchases to one of $C \in \{10, 20, 50, 100\}$ customer groups.
COLLAB [34]	Unbalanced dataset. $C = 3$ and 5, 000 records. Each record represents a graph with 74 nodes and 2, 458 edges on average. The longest graph persists of 2, 000 nodes.	Graph Convolutional Network [35]	Classify graphs to one of $C = 3$ scientific collaboration networks (e.g., Condensed Matter Physics).
Labeled Faces in the Wild [17]	Unbalanced dataset. For the topmost $C \in \{20, 50\}$ classes the dataset comprises 2, 000 resp. 2, 800 250×250 greyscale images.	VGG-Very-Deep-16 CNN [24]	Classify faces to one of the topmost $C \in \{20, 50\}$ labels (i.e., persons).
Skewed Purchases	Balanced dataset with a train and test skew. Per $C \in \{10, 20, 50, 100\}$ the dataset comprises 200, 000 records and 600 features.	Fully connected NN with two layers ($128 \times C$) [28].	Classify purchases to one of $C \in \{10, 20, 50, 100\}$ customer groups.

mitigation efficiency φ as stated below. Equation (2) requires $prec_{orig} - prec_{base} \neq 0$ and $acc_{orig} - acc_{base} \neq 0$, i.e., the original model is vulnerable to MI and yields meaningful test accuracy.

$$\begin{aligned}
 \varphi &= \frac{\left(\frac{\text{maximum decrease accuracy} - \text{actual decrease accuracy}}{\text{maximum decrease accuracy}} \right)}{\left(\frac{\text{maximum decrease precision} - \text{actual decrease precision}}{\text{maximum decrease precision}} \right)} \\
 &= \frac{\frac{(acc_{orig} - acc_{base}) - (acc_{orig} - acc_{\epsilon})}{acc_{orig} - acc_{base}}}{\frac{(prec_{orig} - prec_{base}) - (prec_{orig} - prec_{\epsilon})}{prec_{orig} - prec_{base}}} \quad (2)
 \end{aligned}$$

φ quantifies the relative loss in accuracy in its numerator and the relative gains in privacy in its denominator for a given privacy parameter ϵ . Hence, φ presents the relative privacy-accuracy trade-off as a ratio which we seek to maximize. When the relative gain in privacy (lower MI precision or MI recall) exceeds the relative loss in accuracy φ will be > 1 . In contrast, if the loss in test accuracy exceeds the gain in privacy φ will be < 1 .

4 Datasets and learning tasks

We evaluate five datasets w.r.t. their achievable privacy-accuracy trade-off under LDP and CDP. Each dataset is summarized in Table 2. The datasets have been used in state-of-the-art literature on membership inference, for graph classification and face recognition tasks.

Texas Hospital Stays The Texas Hospital Stays dataset is an unbalanced dataset (i.e., varying amounts of records per label). Furthermore, the dataset consists of high dimensional binary vectors representing patient health features. Each record within the dataset is labeled with a procedure. The learning task is to train a fully connected neural network for classification of patient features to a procedure. We train and evaluate models for a set of most common procedures $C \in \{100, 150, 200, 300\}$. Depending on the number of procedures the dataset comprises 67, 330 – 89, 815 records and 6, 170 – 6, 382 features. To allow comparison to related work we train the target model on $n = 10, 000$ training records and use the remaining set of records for test data and shadow model training data.

Purchases Shopping Carts This dataset is also unbalanced and consists of binary vectors which represent customer shopping carts. However, a significant difference to the Texas Hospital Stays dataset is that the dimensionality (i.e., number of features) is almost 90% lower. Each vector is labeled with a customer group. Similar to the previous dataset, the learning task is to classify shopping carts to customer groups. The dataset is provided in four variations with varying numbers of different labels: $C \in \{10, 20, 50, 100\}$. The dataset consists of 200, 000 records. For this dataset we sample $n = 6, 000$ training records for the target model and leave the rest for test data and shadow model training. This methodology ensures comparability to related work.

While the previous two datasets represent real world data, they were altered (i.e., post-processed by clustering) by Shokri et al. [28] to evaluate their MI Attack. In addition, the datasets represent very similar learning tasks on high dimensional binary vectors for which simple model architectures suffice. To ensure diversity we consider

two additional datasets for graph- and face classification, which come with complex reference architectures for deep learning. These reference architectures involve convolutional neural networks (CNN) that exploit locality of features. Hitaj et al. [16] found CNNs to be less susceptible to model inversion attacks against training data.

COLLAB The COLLAB dataset [34] consists of undirected social graphs stored as adjacency matrix. Each graph represents the ego-collaboration network of a researcher from one of three different fields, namely *high energy*, *condensed matter* or *astro physics*. The learning problem is to predict the correct research field per researcher from those $C = 3$ labels. We implement the graph classification architecture suggested by Zhang et al. [35] which consists of a Graph Convolution Network (GCN) for feature extraction and a final fully connected classifier. In between these two components, a sort-pooling layer is added to support classification of arbitrary graph sizes which we require to classify collaboration networks of different sizes from the COLLAB dataset. However, we omit the final dropout layer. Their model requires an adjacency matrix, a degree vector and a node feature matrix as inputs per graph. As COLLAB provides only adjacency matrices, we reuse the node degrees as feature vector to compensate for missing node feature matrices. The complete dataset contains 5,000 entries with no separation into train and test splits. We choose to split all records into sets of 3,500 training instances and 1,500 testing examples. The maximum edge degree is 2,000. For LDP we randomize all entries in the adjacency matrices with randomized response. This LDP approach achieves edge-local differential privacy, the plausible deniability of any connection within a graph. Randomized adjacency matrices are post-processed by modifying it such that every node has at least one edge to another node and it is symmetric. Yet, this might leave us with unconnected subgraphs.

Labeled Faces in the Wild The Labeled Faces in the Wild (LFW) [17] dataset contains labeled images each depicting a specific person with a resolution of 250×250 pixels. The dataset has a long distribution tail w.r.t. to the number of images per label. We thus focus on learning the $C = 20$ and $C = 50$ classes with the highest number of records in the dataset and transform all images to greyscale. We start our comparison of LDP and CDP from a pre-trained VGG-Very-Deep-16 CNN faces model [24] by keeping the convolutional core, exchanging the dense layer at the end of the model and training for LFW greyscale faces. For LDP, we apply differentially private image pixelation within neighborhood $m = \sqrt{250 \times 250}$ and avoid coarsening by setting $b = 1$. The pre-trained VGG is then trained on LDP images from the training dataset. For CDP we use the DP-Adam optimizer.

Skewed Purchases³ We specifically crafted this dataset to mimic a situation for transfer learning, i.e., the application of a trained model to novel data which is similar to the training data w.r.t. format but following a different distribution. This situation arises for Purchases Shopping Carts, if for example not enough high-quality shopping cart data for a specific retailer are available yet. Thus, only few high-quality data (e.g., manually crafted examples) can be used for testing and large amounts of low quality data from potentially differing distributions for training (e.g., from other retailers). In effect the distribution between train and test data varies for this dataset. Similar to Purchases Shopping Carts the dataset consists of 200,000 records with 600 features and is available in four versions with $C \in \{10, 20, 50, 100\}$ labels. However, each vector x in the training dataset X is generated by using two independent random coins to sample a value from $\{0, 1\}$ per position $i = 1, \dots, 600$. The first coin steers the probability $\Pr[x_i = 1]$ for a fraction of 600 positions per x . We refer to these positions as indicator bits (*ind*) which indicate products frequently purchased together. The second coin steers the probability $\Pr[x_i = 1]$ for a fraction of $600 - \binom{600}{|C|}$ positions per x . We refer to these positions as noise bits (*noise*) that introduce scatter in addition to *ind*. We let $\Pr_{ind}[x_i = 1] = 0.8 \wedge \Pr_{noise}[x_i = 1] = 0.2$, $\forall x \in X_{train}$, and $\Pr_{ind}[x_i = 1] = 0.8 \wedge \Pr_{noise}[x_i = 1] = 0.5$, $\forall x \in X_{test}$, $1 \leq i \leq 600$. This dataset has a difference in information entropy between test and train data of ≈ 0.3 . The difference would be ≈ 0 , if there is no skew. Figure 3 depicts the MI precision over the different training dataset distributions and a fixed test distributions, and illustrates that datasets with varying train and test distributions are actually more vulnerable to MI and thus potentially require stronger privacy parameters.

5 Experiments

We perform a single experiment per dataset. The experiment compares LDP and CDP under MI precision and recall instead of privacy parameter ϵ . The experiment is analyzed through three sets of figures. First, by plotting test accuracy and MI precision and recall over ϵ , respectively. The three resulting graphs map ϵ to MI precision and recall, and test accuracy. We present this information for CDP per dataset in figures 4–8a,b,c and for LDP in figures 4–8e,f,g. Second, by comparing the achievable MI precision and recall over target model test accuracy in a scatterplot to identify of strictly better privacy-accuracy trade-offs per dataset. We present this information for LDP and CDP per dataset in

³We provide this dataset on GitHub: Blinded repository.

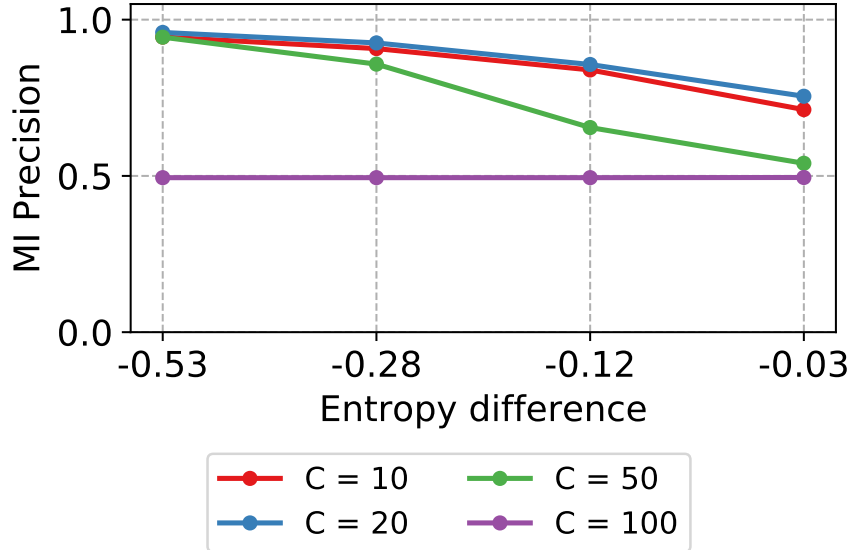


Figure 3: Skewed Purchases skew effect on MI precision

Table 3: Overview of LDP ϵ .

Dataset	LDP composed ϵ	Comment
Texas Hospital Stays	51,000 – 638	$6,382 \times \epsilon_i$
Purchases	4,800 – 60	$600 \times \epsilon_i$
COLLAB	16,000 – 200	$2,000 \times \epsilon_i$
LFW	62.5×10^6 – 6,250	$250 \times 250 \times \epsilon_i$
Skewed Purchases	4,800 – 60	$600 \times \epsilon_i$

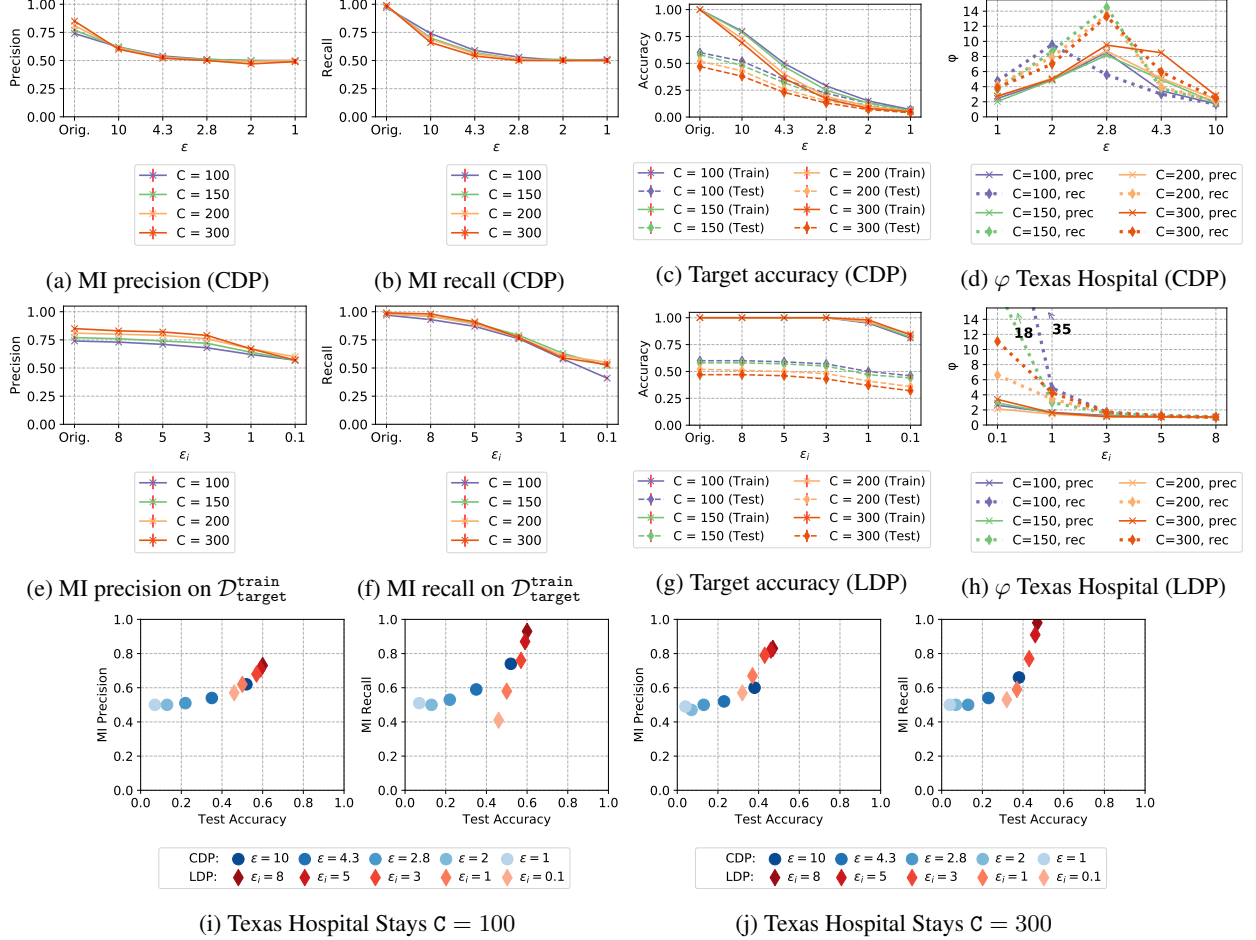
figures 4–8i,j. Third, by calculating φ (cf. Equation (2) in Section 3.2) to identify efficient privacy parameters for $\mathcal{D}\mathcal{O}$ w.r.t. mitigating MI precision. The corresponding figures are 4–8d for CDP and 4–8h for LDP.

For all executions of the experiment CDP noise is sampled from a Gaussian distribution (cf. Definition 3) with $\sigma = \text{noise multiplier } z \times \text{clipping norm } C$. We evaluate increasing noise regimes per dataset by evaluating noise multipliers $z \in \{2, 4, 6, 8, 16\}$ until model convergence per dataset and calculate the resulting ϵ at a fixed $\delta = \frac{1}{n}$. We denote the non-private, original MI precision and $\mathcal{D}\mathcal{O}$ test accuracy as *original*. For LDP we use the same hyperparameters as in the original training and evaluate two local randomizers, namely randomized response and LDP image pixelation with the Laplace mechanism. For each randomizer we state the individual ϵ_i per invocation (i.e., per anonymized value) and ϵ per record (i.e., collection of dependent values). We apply randomized response to all datasets except LFW with a range of privacy parameter values $\epsilon_i \in \{0.1, 1, 3, 5, 8\}$ that reflect varying retention probabilities. For LFW we perturb each pixel with Laplace noise, and also investigate a wide range of resulting noise regimes by varying ϵ_i . For ease of reading we provide the composed ϵ for LDP per dataset in Table 3. Each experiment has been stabilized over five independent executions. We provide hyper-parameters for all experiments in Table 4. Since we want to measure privacy w.r.t. original data, we solely show LDP results on $\mathcal{D}_{\text{target}}^{\text{train}}$ instead of $\mathcal{L}\mathcal{R}(\mathcal{D}_{\text{target}}^{\text{train}})$ for all experiments.

Texas Hospital Stays For Texas Hospital Stays we achieve an original target model test accuracy between ≈ 0.45 – 0.65 and MI precision between 0.75 – 0.85 depending on C . The use of DP-SGD with increasing noise multipliers results in privacy guarantees $\epsilon \in \{10, 4.3, 2.8, 2, 1\}$. The MI precision and recall, and target model accuracies, over ϵ are depicted in Figures 4a, 4b, and 4c for CDP. A first observation is that the drop in $\mathcal{D}\mathcal{O}$ ’s test accuracy is less steep than the drop in train accuracy. Furthermore, the decrease in accuracy is similar for any classification task C . However, it is observable that already at $\epsilon = 2$ the test accuracy is close to the baseline of uniform guessing. For \mathcal{A} ’s MI precision and recall we can observe that low ϵ are indeed not required since nearly perfect mitigation of both is achieved at $\epsilon = 4.3$ for all C . However, $\mathcal{D}\mathcal{O}$ indeed is paying a significant price for achieving mitigation since test accuracies are nearly cut in half over at $\epsilon = 4.3$.

Table 4: Hyperparameters

C		Texas Hospital Stays				Purchases Shopping Carts				GCN	LFW			Skewed Purchases			
C		100	150	200	300	10	20	50	100	3	20	50	10	20	50	100	
Learning rate	Baseline	0.1	0.1	0.1	0.1	0.1	0.1	0.1	0.1	10^{-4}	10^{-3} to 8×10^{-4}	4×10^{-4} to 8×10^{-4}	10^{-3}	10^{-3}	10^{-3}	10^{-3}	
	CDP	0.01	0.01	0.01	0.01	0.1	0.1	0.1	0.1	10^{-3}	10^{-3}	10^{-3}	10^{-3}	10^{-3}	10^{-3}	10^{-3}	
	LDP	0.1	0.1	0.1	0.1	0.1	0.1	0.1	0.1	10^{-4}	10^{-3}	10^{-3}	10^{-3}	10^{-3}	10^{-3}	10^{-3}	
Batch Size	Baseline	128	128	128	128	128	128	128	128	50	32	32	100	100	100	100	
	CDP	128	128	128	128	128	128	128	128	50	16	16	100	100	100	100	
	LDP	128	128	128	128	128	128	128	128	50	32	32	100	100	100	100	
Epochs	Baseline	200	200	200	200	200	200	200	200	300	30	30	200	200	200	200	
	CDP	1000	1000	1000	1000	200	200	200	200	100	110	110	200	200	200	200	
	LDP	200	200	200	200	200	200	200	200	300	30	30	200	200	200	200	

Figure 4: \mathcal{DO} accuracy and privacy analysis on the Texas Hospital Stays (error bars lie within most points)

For LDP via randomized response \mathcal{DO} 's target model test accuracies over ϵ_i are presented in Figure 4g. LDP also affects all classification tasks C similar and, compared to CDP, achieves a lower slope for the decrease of \mathcal{DO} 's test accuracy over ϵ_i . However, The use of randomized response does not keep-up with the use of DP-SGD w.r.t. \mathcal{DO} 's privacy. Figure 4e and 4f depict \mathcal{A} 's MI precision and outline that MI is only nearly mitigated at a small $\epsilon_i = 0.1$.

We provide a scatterplot of LDP and CDP MI precision and recall against test accuracy for the smallest classification task $C = 100$ and the largest classification task $C = 300$ in Figure 4i and 4j. Here, superior combinations of MI recall and test accuracy are achieved for LDP, while the points for MI precision and test accuracy are similar. Consequently, we observe from Figure 4h and 4d that the relative privacy-accuracy trade-off for LDP exceeds CDP efficiency in w.r.t. MI recall with $\varphi \approx 35$ and 20 for $C = 100$ and 150. The privacy-accuracy trade-off for LDP and CDP MI precision and recall is most efficient from $\epsilon_i = 0.1$ to 1 and $\epsilon = 2$ to 2.8, respectively.

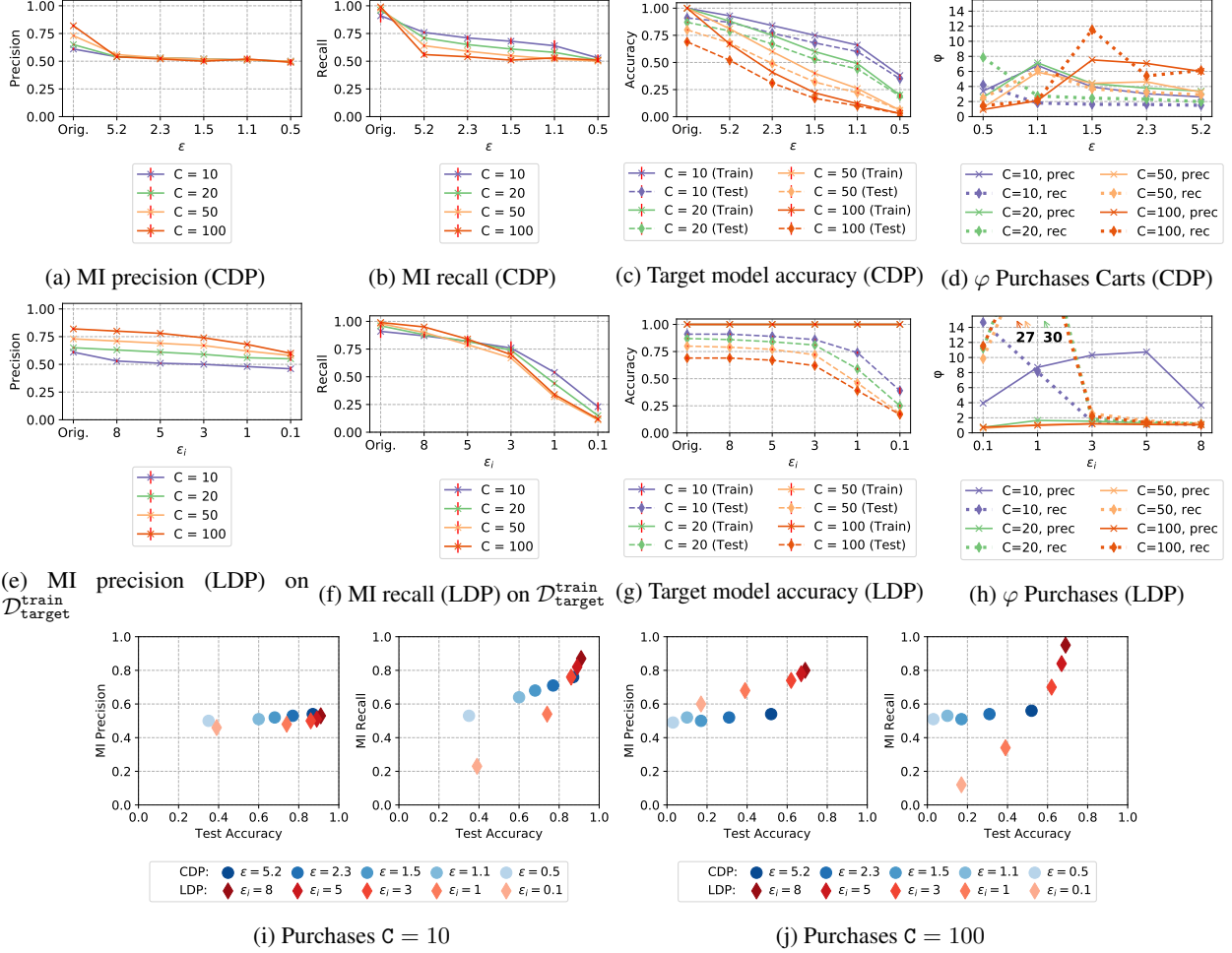


Figure 5: \mathcal{DO} accuracy and privacy analysis on the Purchases Shopping Carts (error bars lie within most points)

Purchases Shopping Carts We state the CDP MI precision and recall, and target model accuracy in figures 5a, 5b and 5c. For the Purchases dataset the DP-SGD noise multiplies result in $\epsilon \in \{5.2, 2.3, 1.5, 1.1, 0.5\}$. Nearly perfect mitigation of MI precision and recall is achieved already at $\epsilon = 5.2$, and any $\epsilon < 5.2$ only lowers \mathcal{A} 's MI recall. Thus, \mathcal{A} increasingly refrains from labeling records as “in” as the classification confidence values decrease over ϵ . Again, the decreases in test accuracy are similar for all classification C .

Figures 5e and 5f depict the LDP MI Precision and recall. Both are lowered only slightly over decreasing ϵ_i for $\mathcal{D}_{\text{train}}^{\text{target}}$. Finally, reasonable MI mitigation is achieved at $\epsilon_i = 0.1$. We again present the test accuracies over ϵ_i for randomized response in Figure 5g. The slope of decrease in test accuracy is small in contrast to the DP-SGD until $\epsilon_i = 3$, and then increases significantly for $\epsilon_i < 3$. Thus, leading to poor test accuracies under this privacy regime.

We illustrate MI precision and recall arranged in scatterplots for $C = 10$ and $C = 100$ in Figure 5i and 5j. While LDP in contrast to CDP yields lower MI precision at similar test accuracy for $C = 10$, CDP is becoming superior w.r.t. to MI precision as the complexity of the classification task grows to $C = 100$. In contrast, the privacy-accuracy trade-off for MI recall is superior under LDP for $C = 10$ and $\epsilon \leq 3$, and $C = 100$ for $\epsilon < 3$.

The relative privacy-accuracy trade-off for CDP is depicted in Figure 5d. Two efficiency optima for φ can be observed: for $C \in \{10, 20, 50\}$ and $C = 100$. While the main decrease in \mathcal{A} 's MI precision is already occurring for high ϵ , and φ is high in general, the two efficiency optimal ϵ configurations still provide test accuracies well above the baseline and further decrease \mathcal{A} 's MI precision. A more stronger differentiation between low and high C is occurring under LDP as depicted in Figure 5h. For MI precision all $C \neq 10$ remain close to $\varphi = 1$ due to the comparatively higher MI Precision and lower test accuracy. In contrast, for MI recall increases over ϵ_i , peaking at $\varphi \approx 30$ for $\epsilon_i = 1$ and $C \geq 20$.

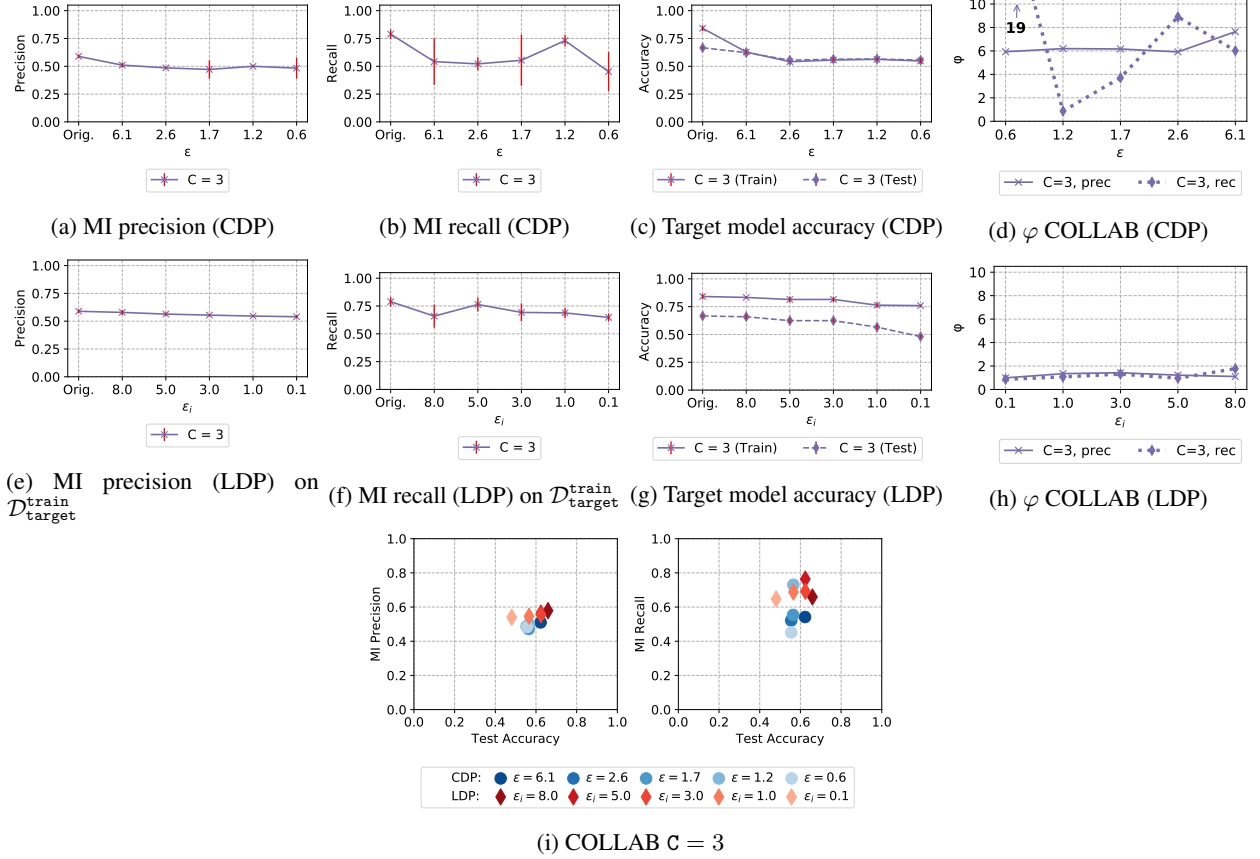
Figure 6: \mathcal{DO} accuracy and privacy analysis on COLLAB

Table 5: Privacy parameters for DP-ADAM on LFW

	CDP ϵ for $z \in \{1, 2, 4, 8, 16\}$
$C = 20$	$\epsilon \in \{4.8, 2.1, 1.3, 1.0, 0.5\}$
$C = 50$	$\epsilon \in \{3.9, 1.7, 1.1, 0.8, 0.4\}$

COLLAB The reference architecture results in a target model test accuracy of 0.65, and MI precision and recall of ≈ 0.6 and ≈ 0.75 , respectively. The use of the DP-Adam optimizer on this dataset results in $\epsilon \in \{6.1, 2.6, 1.7, 1.2, 0.6\}$ for CDP. Again, MI precision and recall, and target model accuracies are presented by figures 6a, 6b and 6c. The MI precision gets diminished to ≈ 0.5 already at the second smallest noise multiplier with $\epsilon = 2.6$. Furthermore, MI recall is reduced to the baseline at 0.5 over all privacy parameters except $\epsilon = 1.2$, which consistently produces an outlier. However, there is an observable trend over ϵ .

The LDP MI precision and recall, and target model accuracies are depicted on figures 6e, 6f and Figure 6g. LDP neither reaches the baseline for MI precision nor recall even with the a small $\epsilon_i = 0.1$. However, at this privacy parameter LDP results in a large decrease of test accuracy. MI recall is comparably more unstable, and only decreases slightly over ϵ_i .

The scatterplots in Figure 6i underline that for this dataset CDP yields lower MI precision and recall at similar test accuracy for almost all datapoints. We account this to the comparatively weak privacy notion of edge local differential privacy that was achieved under LDP. Figure 6d and 6h state φ for CDP and LDP. Here, CDP and LDP ϵ and ϵ_i only have a small, quickly converging effect on MI precision and recall and consequently \mathcal{DO} can argue to select high ϵ , ϵ_i .

LFW We have to diverge from previous experiments for the calculation of CDP ϵ for this dataset since the training data n for $C = 50$ is larger than for $C = 20$, and thus the same noise multiplier results in lower ϵ for $C = 50$. We state the corresponding privacy parameters ϵ in Table 5.

For CDP with DP-Adam Figure 7a states \mathcal{A} 's MI precision. Here, we mainly observe differences between $C = 50$ and $C = 20$ w.r.t. the original MI precision. While for $C = 20$ the original MI precision is initially at the baseline and

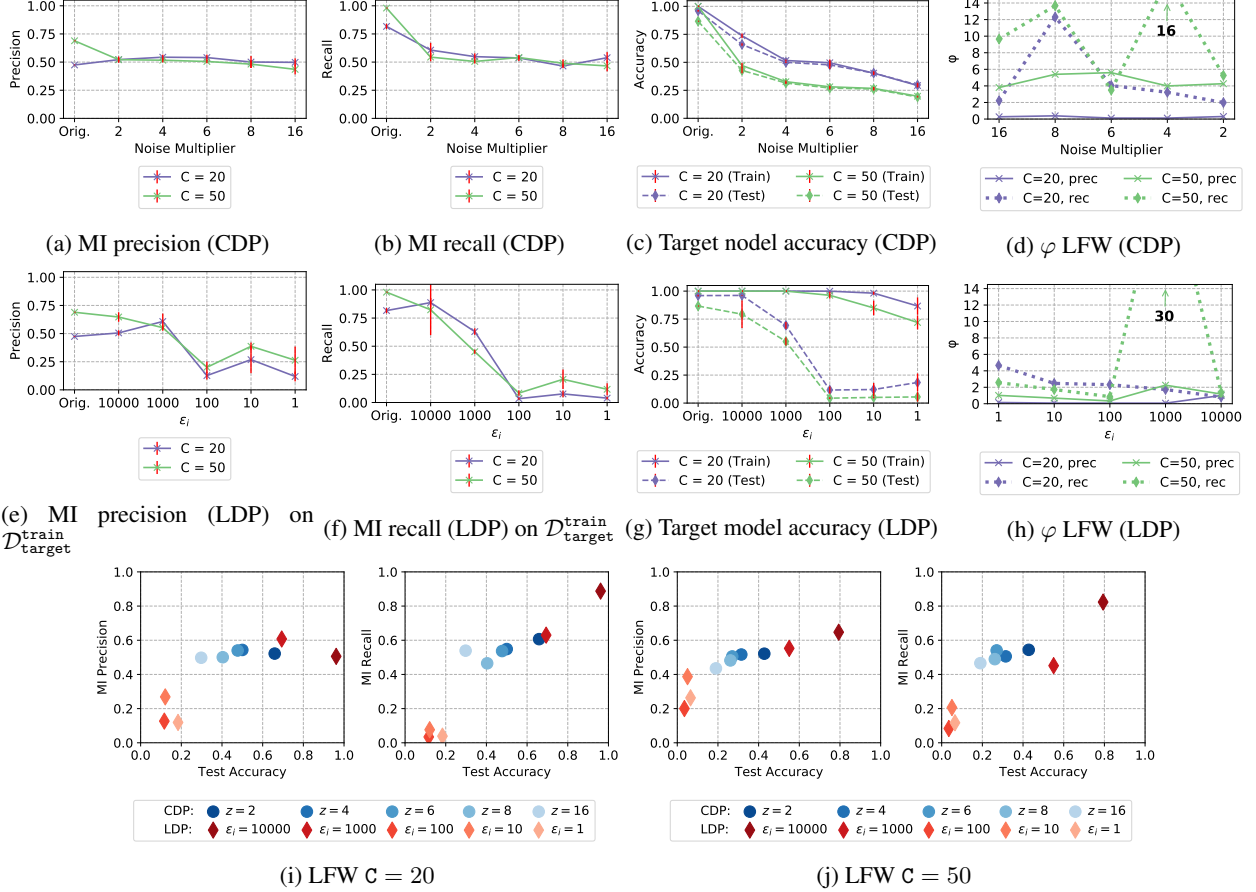


Figure 7: \mathcal{DC} accuracy and privacy analysis on LFW

slightly increases for small noise regimes. In contrast we notice the effect of a larger training set size n for $C = 50$ where the baseline MI precision is close to 0.7 and already overcome at a low privacy regime. This effect is amplifying even more for larger C , which we however omit due to space constraints. \mathcal{A} 's recall is stated in Figure 7b and initially high for $C=20$ and 50 at ≈ 0.75 and ≈ 1.0 , respectively. CDP already decreases the number of true positives already for high ϵ . Figure 7c states the target model train and test accuracy over the previously introduced noise regimes. We see that CDP closes the test-train gap for both datasets already at small noise regimes (i.e., high ϵ). Furthermore, the initially large drop in both train and test accuracy is converging fast and even at high privacy regimes (i.e., low ϵ) the models for $C = 20$ and $C = 50$ stay well above their baseline accuracies.

We again present the LDP MI precision and recall over ϵ_i in figures 7e and 7f. MI precision and recall are lowered significantly below their respective baselines over ϵ_i , an effect which we did not observe for any dataset before. The fact that \mathcal{A} indeed does achieve higher MI precision and recall when executing an MI Attack against $\mathcal{LR}(\mathcal{D}_{\text{target}}^{\text{train}})$ instead of $\mathcal{D}_{\text{target}}^{\text{train}}$ leads us to assume that the MI Attack applied by \mathcal{A} learned to exploit false features during training due to the change between train and test data caused by the application of LDP on the images. However, the MI attack against $\mathcal{LR}(\mathcal{D}_{\text{target}}^{\text{train}})$ is not reflecting an accurate privacy evaluation w.r.t. original training records.

For LDP target model accuracies in Figure 7g we indeed observe that the structural change which LDP image pixelation causes leads to quick losses in test accuracy and a widening train-test-gap. This gap closes again only at very strong perturbation at $\epsilon_i \leq 10$.

In the scatterplots provided in Figure 7i and 7j for $C = 20$ and 50 we observe that LDP spans a more favorable curve for MI recall. We state the CDP φ in Figure 7d. Due to the low baseline for $C = 20$ we observe $\varphi < 1$ for MI precision throughout all noise multipliers. However, we indeed observe that MI recall is efficiently mitigated for $C = 20$, with the CDP MI recall efficiency peak at $\varphi \approx 16$ for noise multiplier 8. In contrast, for $C = 50$ φ indeed supports \mathcal{DC} for MI precision and recall by pointing out that the most efficient choices are already realized between the noise multipliers 4 and 6 for MI precision and MI recall. Note that $\varphi = 16$ for MI recall. Figure 7h depicts the relative privacy-accuracy

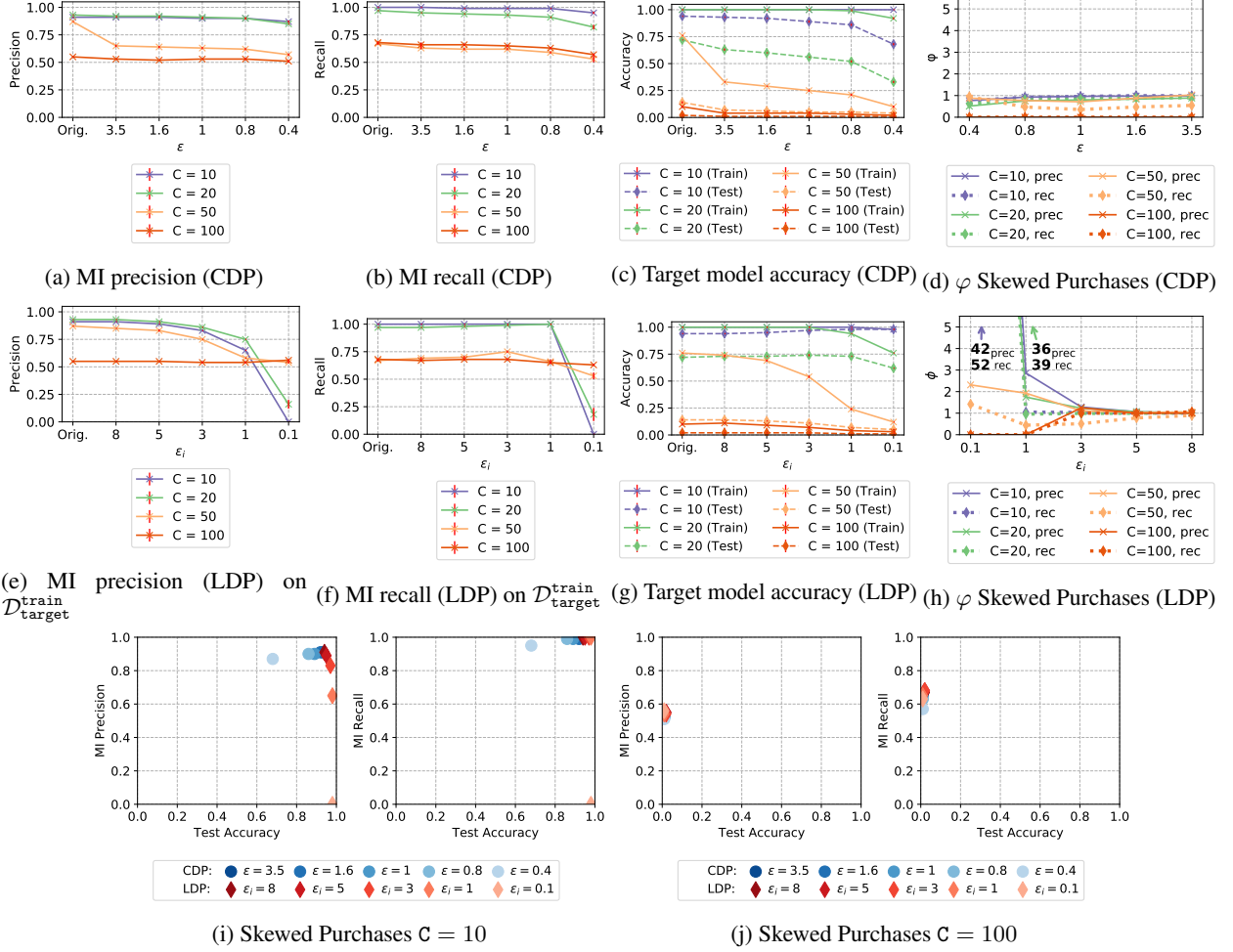


Figure 8: \mathcal{DO} accuracy and privacy analysis on Skewed Purchases (error bars lie within most points)

trade-off for LDP. Since test accuracy actually slightly increases for $C = 20$ and MI precision remains at baseline under $\epsilon_i = 10,000$ φ is initially acceptable. For $C = 50$ efficient ϵ are observed for $\epsilon_i = 1,000$, where $\varphi \approx 30$ for MI recall and thus even exceeds CDP.

Skewed Purchases The effect which we observed for LDP on the LFW dataset let us to further analyze differing distributions between train and test data. This effect is for example encountered when insufficient high-quality data for training is initially available and reference data that potentially follows a different distribution has to be acquired for first training. In comparison to Purchases Shopping Carts CDP results in stronger privacy guarantees $\epsilon \in \{3.5, 1.6, 1, 0.8, 0.4\}$ which are due to differences in batch size and training epochs between both datasets.

Figure 8a states the changes in MI precision over privacy guarantees ϵ . While for the simple classification tasks $C \in \{10, 20\}$ MI precision remains at the original even over all ϵ , for $C = 50$ MI precision drops close to the baseline at 0.53 already for $\epsilon = 3.5$. In contrast, ϵ has only a small effect on MI recall as depicted in Figure 8b. The baseline is solely reached for $C \in \{50, 100\}$ at $\epsilon = 0.4$. Figure 8c presents target model accuracies over ϵ . The decrease in test accuracy is comparatively stronger for $C \in \{10, 20\}$ due to the low initial baseline for $C \in \{10, 20\}$. CDP comes indeed at a heavy cost on this dataset: DP-SGD weakens \mathcal{A} 's MI precision while significantly lowering \mathcal{DO} 's test accuracy.

We state MI Precision and recall for over ϵ_i for LDP in Figures 8e and 8f. While MI precision is not much affected for $C \neq 100$ until $\epsilon_i = 1$, MI recall is solely affected by LDP at a strong $\epsilon_i = 0.1$ and $C \in \{10, 20\}$.

Figure 8g indicates that \mathcal{DO} 's test accuracy in LDP is robust to noise under randomized response especially for classification tasks for which n is much larger than the dimensionality l of the training data per class (e.g., $C \in \{10, 20\}$). For $C \in \{10, 20\}$ randomized response solely affects \mathcal{DO} 's test accuracy under a strong $\epsilon_i = 0.1$ in contrast to

Table 6: MI precision: comparison of lower and upper ϵ and ϵ_i for which $\varphi > 1$

		Texas Hospital Stays				Purchases Shopping Carts				GCN	LFW		Skewed Purchases			
C		100	150	200	300	10	20	50	100	3	20	50	10	20	50	100
LDP	lower ϵ_i	0.1	0.1	0.1	0.1	0.1	1	1	1	1	n/a	1,000	0.1	0.1	0.1	3
	upper ϵ_i	3	3	3	3	8	8	8	8	5	n/a	10,000	5	5	5	5
CDP	lower ϵ	1	1	1	1	0.5	0.5	1.1	1.1	0.6	n/a	0.4	n/a	n/a	n/a	n/a
	upper ϵ	10	10	10	10	5.2	5.2	5.2	5.2	6.1	n/a	3.9	n/a	n/a	n/a	n/a

Table 7: MI recall: comparison of lower and upper ϵ and ϵ_i for which $\varphi > 1$

		Texas Hospital Stays				Purchases Shopping Carts				GCN	LFW		Skewed Purchases			
C		100	150	200	300	10	20	50	100	3	20	50	10	20	50	100
LDP	lower ϵ_i	0.1	0.1	0.1	0.1	0.1	0.1	0.1	0.1	1 and 5	1, 100	0.1	0.1	n/a	n/a	
	upper ϵ_i	5	5	5	5	8	8	8	8	3, 8	10, 1000	1	1	n/a	n/a	
CDP	lower ϵ	1	1	1	1	0.5	0.5	0.5	0.5	0.6	0.5	0.4	n/a	n/a	n/a	n/a
	upper ϵ	10	10	10	10	5.2	5.2	5.2	5.2	6.1	4.8	3.9	n/a	n/a	n/a	n/a

$C \in \{50, 100\}$ at $\epsilon_i = 5$. For $C \in \{10, 20\}$ we observe a regularization effect from randomized response which generalizes $\mathcal{D}_{\text{target}}^{\text{train}}$ towards $\mathcal{D}_{\text{target}}^{\text{test}}$. Here, the test-train-gap narrows due to increasing test accuracy. Thus, the confidence values also become similar and impede \mathcal{A} 's attack model in distinguishing predictions from $\mathcal{D}_{\text{target}}^{\text{train}}$ and $\mathcal{D}_{\text{target}}^{\text{test}}$. Finally resulting in a decreasing MI recall.

Again we provide scatterplots for $C = 10$ and 100 in Figure 8i and 8j. A meaningful relative privacy-accuracy trade-off for MI precision and recall is only achieved under LDP for under $C = 10$ and 20 . For $C = 10$, $\epsilon_i = 0.1$ LDP trumps $\epsilon = 3.5$ CDP. Figure 8d illustrates that Skewed Purchases is the only dataset where almost all $\varphi \leq 1$ for MI recall and precision under CDP. This observation supports our first impression that CDP impacts $\mathcal{D}\mathcal{O}$'s test accuracy stronger than \mathcal{A} 's MI precision and recall. For LDP we observe high φ in Figure 8h for $C \in \{10, 20\}$ and strong $\epsilon_i \leq 1$. $\varphi \approx 50$ for MI recall at $\epsilon_i = 0.1$. However, these high efficiency values are mainly due to an increasing test accuracy over ϵ_i at small decreases in MI recall and precision.

6 Discussion

In the following we formulate findings based on the results from our experiment.

Privacy parameter ϵ alone is unsuited to compare and select mechanisms We consistently observed that while ϵ in LDP is higher by a factor of hundreds or even thousands in comparison to CDP, the protection against \mathcal{A} 's MI precision is actually not considerably weaker. For instance, the minimal MI precisions for Texas Hospital Stays are within a distance of 0.1 for all C at CDP $\epsilon = 1$ and LDP $\epsilon = 683$. For Purchases Shopping Carts the MI precision is for example equivalent for LDP and CDP on $C = 10$, and only slightly higher for LDP on $C = 100$, at CDP $\epsilon = 1.1$ and LDP $\epsilon = 60$. We also observed a similar combination of MI precision and test accuracy on LFW at $C = 50$ for the privacy parameters $\epsilon = 2$ CDP and $\epsilon = 62.5 \times 10^5$ LDP. Thus, we note that assessing privacy solely based on ϵ falls short. Given the results of the previous sections we would rather encourage data scientists to communicate risk measured under a specific threat model, such as membership inference, in addition to privacy parameter ϵ .

LDP and CDP result in differing privacy-accuracy curves Our methodology allowed us to evaluate a wide area of privacy regimes in CDP and LDP. We observed for most datasets that the resulting privacy-accuracy combinations are very different for LDP and CDP. Furthermore, we observed for Texas Hospital Stays, Purchases Shopping Carts and LFW that MI recall is comparatively lower at similar test accuracy for LDP. For instance, for Purchases Shopping Carts we observe comparatively better MI recall and test accuracy combinations for LDP between LDP $\epsilon = 1, 800$ and $\epsilon = 60$ than we do for most CDP ϵ . The same observation holds for Texas Hospital Stays at LDP $\epsilon \leq 18,000$ and $\leq 6, 830$ for $C = 100$ and 300 , respectively. Also, LDP yields comparatively lower MI recalls for LFW at $\epsilon \leq 1, 000$.

The relative privacy-accuracy trade-off is favorable within a small interval Table 6 and 7 present summaries of lower and upper ϵ and ϵ_i between which $\varphi > 1$ w.r.t. MI precision and recall, respectively. While the lower and upper boundaries for MI precision and recall are similar for CDP most intervals are extending between MI precision and recall for LDP. This underlines that the change that LDP causes in the training data distribution especially affects MI recall. For LFW the high variety in the training images even pushed \mathcal{A} 's MI precision and recall below baseline.

Note that for $\varphi \gg 1$, which we assume to be a requirement for the use of either LDP or CDP in learning tasks with demand for high test accuracy and low MI precision or recall, the interval between lower and upper ϵ and ϵ_i is becoming drastically shorter for all datasets, if achievable at all. In the course of this work observed MI precision $\varphi \gg 1$ mainly

for CDP, with the exception of Skewed Purchases and LFW $C = 20$ where $\varphi > 1$ (i.e., decreasing MI precision more than test accuracy) could not be achieved. In contrast, for MI recall we observed $\varphi \gg 1$ more often under LDP.

Privacy decay and ensemble learning Note that we trained a single target model within this work and did not empirically evaluate ensembles of models which are found in practice. In such ensembles the attack surface would widen from a single target model to all ensemble target models. Furthermore, the privacy loss would also accumulate over all ensemble target models when assuming that training data is reused between ensemble models. Here, we see one architectural benefit of LDP: flexibility. LDP training data can be used for all ensemble models without widening the attack surface in contrast to CDP.

7 Related Work

Our work is related to differentially private neural networks, attacks against the confidentiality of the underlying training data of machine learning models, and interpretation of the privacy parameter ϵ in neural network training.

CDP is a common approach to realize differentially private neural networks by adding noise to the gradients during model training. Foundational approaches for perturbation with the differentially private gradient descent during model training were provided by Song et al. [29] and Bassily et al. [3]. Shokri et al. [27] formulate a protocol for federated learning with CDP where multiple participants improve a global model locally on their own data and share perturbed gradient updates. A potential limitation of their federated learning protocol is that noise is added per parameter, leading to high ϵ . Abadi et al. [1] introduce the Moments Accountant composition theorem and suggest a novel implementation of the DP-SGD, which in combination allow model training under a modest privacy budget.

Fredrikson et al. [11, 12] formulate model inversion attacks that uses target model softmax confidence values to reconstruct training data per class. The reconstructed data represents crafted training examples that are classified with high confidence, i.e., training examples carrying the identifying (average) features for a given class. In contrast, MI attacks address the threat of identifying individual records in a dataset (e.g., [26, 2]). Hayes et al. [15] contribute MI attacks against generative adversarial models. Similar to our work they evaluate DP as mitigation. While we use LDP and CDP for feedforward neural networks their work addresses generative models and suggests to apply CDP at the discriminator. Shokri et al. [22] formulate an optimal mitigation against their MI attack [28] by using adversarial regularization. By applying the MI attack gain as a regularization term to the objective function of the target model, a non-leaking behavior is enforced w.r.t. MI. While their approach protects against their MI adversary, DP mitigates any adversary with arbitrary background information.

Carlini et al. [5] suggest *exposure* as a metric to measure the extend to which neural networks memorize sensitive information. Similar to our work, they apply DP for mitigation. We agree that the desire to measure memorization of secrets is promising, however, in this work we focus on attacks against machine learning models targeting identification of members of the training dataset. In an empirical study, Rahman et al. [25] applied the black-box MI attack against DP-SGD models to CIFAR-10 and MNIST. We additionally consider LDP and a wider rider range of datasets. In contrast to our work Rahman et al. evaluate the severity of MI attack by MI accuracy and the F1-score which results in numerically higher scores. The difference becomes visible for MI scores on MNIST. Whereas Shokri et al. [28] identify MNIST models to be robust against MI for $n \geq 10,000$ (i.e., MI precision $\approx .0.5$), Rahman et al. argue for MI vulnerability since MI accuracy and F1-score are above baseline.

8 Conclusion

This work compared local and central differential privacy mechanisms for differentially private deep learning under a membership inference threat model. The privacy-accuracy comparison comprises membership inference precision and recall, and test accuracy, to support data scientists in choosing among available DP mechanisms and selecting privacy parameter ϵ . Our experiments on diverse learning tasks show that neither local differential privacy nor central differential privacy yields a consistently better privacy-accuracy trade-off. Thus, when having the choice data scientists should compare the privacy-accuracy trade-off for LDP and CDP per dataset. We furthermore suggest to consider the relative privacy-accuracy trade-off for LDP and CDP as the ratio of losses in accuracy and privacy over privacy parameters ϵ , and show that it is only favorable within a small interval.

9 Acknowledgements

This work has received funding from the European Union’s Horizon 2020 research and innovation program under grant agreement No. 825333 (MOSAICROWN).

References

- [1] M. Abadi, A. Chu, I. Goodfellow, H. B. McMahan, I. Mironov, K. Talwar, and L. Zhang. Deep Learning with Differential Privacy. In *Proc. of Conference on Computer and Communications Security (CCS)*, 2016.
- [2] M. Backes, P. Berrang, M. Humbert, and P. Manoharan. Membership Privacy in MicroRNA-based Studies. In *Proc. of Conference on Computer and Communications Security (CCS)*, 2016.
- [3] R. Bassily, A. Smith, and A. Thakurta. Private Empirical Risk Minimization. In *Proc. of Symposium on Foundations of Computer Science (FOCS)*, 2014.
- [4] BBC News. Google DeepMind NHS app test broke UK privacy law, 07 2017.
- [5] N. Carlini, C. Liu, J. Kos, Ú. Erlingsson, and D. Song. The secret sharer: Measuring unintended neural network memorization and extracting secrets. *ArXiv*, 2018.
- [6] C. Dwork. Differential Privacy. In *Proc. of Colloquium on Automata, Languages and Programming (ICALP)*, 2006.
- [7] C. Dwork, K. Kenthapadi, F. McSherry, I. Mironov, and M. Naor. Our Data, Ourselves. In *Proc. of Conference on Theory and Applications of Cryptographic Techniques (EUROCRYPT)*, 2006.
- [8] C. Dwork and A. Roth. The Algorithmic Foundations of Differential Privacy. *Foundations and Trends in Theoretical Computer Science*, 2014.
- [9] U. Erlingsson, V. Pihur, and A. Korolova. RAPPOR: Randomized Aggregatable Privacy-Preserving Ordinal Response. In *Proc. of Conference on Computer and Communications Security (CCS)*, 2014.
- [10] L. Fan. Image pixelization with differential privacy. In *Proc. of Conference on Data and Applications Security and Privacy (DBSEC)*, 2018.
- [11] M. Fredrikson, S. Jha, and T. Ristenpart. Model Inversion Attacks that Exploit Confidence Information and Basic Countermeasures. In *Proc. of Conference on Computer and Communications Security (CCS)*, 2015.
- [12] M. Fredrikson, E. Lantz, S. Jha, S. Lin, D. Page, and T. Ristenpart. Privacy in Pharmacogenetics: An End-to-End Case Study of Personalized Warfarin Dosing. In *Proc. of USENIX Security Symposium*, 2014.
- [13] I. Goodfellow, Y. Bengio, and A. Courville. *Deep Learning*. MIT Press, 2016. <http://www.deeplearningbook.org>.
- [14] Y. Grandvalet and S. Canu. Comments on “Noise injection into inputs in back propagation learning”. *IEEE Transactions on Systems, Man, and Cybernetics*, 1995.
- [15] J. Hayes, L. Melis, G. Danezis, and E. De Cristofaro. LOGAN: Membership Inference Attacks Against Generative Models. *Proc. on Privacy Enhancing Technologies (PoPETs)*, 2019.
- [16] B. Hitaj, G. Ateniese, and F. Perez-Cruz. Deep models under the gan: Information leakage from collaborative deep learning. In *Proc. of Conference on Computer and Communications Security (CCS)*, 2017.
- [17] G. B. Huang, M. Ramesh, T. Berg, and E. Learned-Miller. Labeled faces in the wild: A database for studying face recognition in unconstrained environments. In *Technical Report 07-49*. University of Massachusetts, 2007.
- [18] P. Kairouz, S. Oh, and P. Viswanath. The Composition Theorem for Differential Privacy. *IEEE Transactions on Information Theory*, 2017.
- [19] S. P. Kasiviswanathan, H. K. Lee, K. Nissim, S. Raskhodnikova, and A. Smith. What can we learn privately? *SIAM Journal on Computing*, 2008.
- [20] K. Matsuoka. Noise injection into inputs in back-propagation learning. *IEEE Transactions on Systems, Man, and Cybernetics*, 1992.
- [21] I. Mironov. Rényi differential privacy. In *Proc. of Computer Security Foundations Symposium (CSF)*, 2017.
- [22] M. Nasr, R. Shokri, and A. Houmansadr. Machine learning with membership privacy using adversarial regularization. In *Proc. of Conference on Computer and Communications Security (CCS)*, 2018.
- [23] N. Papernot, M. Abadi, Ú. Erlingsson, I. Goodfellow, and K. Talwar. Semi-supervised Knowledge Transfer for Deep Learning from Private Training Data. In *Proc. of Conference on Learning Representations (ICLR)*, 2017.
- [24] O. M. Parkhi, A. Vedaldi, and A. Zisserman. Deep face recognition. In *British Machine Vision Conference*, 2015.
- [25] M. A. Rahman, T. Rahman, R. Laganière, and N. Mohammed. Membership inference attack against differentially private deep learning model. *Transactions on Data Privacy*, 2018.

- [26] S. Sankararaman, G. Obozinski, M. I. Jordan, and E. Halperin. Genomic privacy and limits of individual detection in a pool. *Nature Genetics*, 2009.
- [27] R. Shokri and V. Shmatikov. Privacy-preserving Deep Learning. In *Proc. of Conference on Computer and Communications Security (CCS)*, 2015.
- [28] R. Shokri, M. Stronati, C. Song, and V. Shmatikov. Membership inference attacks against machine learning models. In *Proc. of Symposium on Security and Privacy*, 2017.
- [29] S. Song, K. Chaudhuri, and A. D. Sarwate. Stochastic gradient descent with differentially private updates. In *Proc. of Conference on Signal and Information Processing*, 2013.
- [30] F. Tramèr, F. Zhang, A. Juels, M. K. Reiter, and T. Ristenpart. Stealing machine learning models via prediction apis. In *Proc. of USENIX Security Symposium*, 2016.
- [31] T. Wang, J. Blocki, N. Li, and S. Jha. Locally Differentially Private Protocols for Frequency Estimation. In *Proc. of USENIX Security Symposium*, 2017.
- [32] S. L. Warner. Randomized Response: A Survey Technique for Eliminating Evasive Answer Bias. *Journal of the American Statistical Association*, 1965.
- [33] R. Wirth and J. Hipp. Crisp-dm: Towards a standard process model for data mining. In *Proc. of Conference on practical applications of knowledge discovery and data mining*, 2000.
- [34] P. Yanardag and S. Vishwanathan. Deep graph kernels. In *Proc. of Conference on Knowledge Discovery and Data Mining (KDD)*, 2015.
- [35] M. Zhang, Z. Cui, M. Neumann, and Y. Chen. An end-to-end deep learning architecture for graph classification. In *AAAI*, 2018.